Suppression of Impurity Back Scattering in Double Quantum Wires: Theory beyond the Born Approximation

Danhong Huang

Air Force Research Laboratory (AFRL/VSSS), Kirtland Air Force Base, New Mexico 87117

S. K. Lyo

Sandia National Laboratories, Albuquerque, New Mexico 87185

Abstract

The effect of higher-order corrections to the Born approximation is studied for the previously obtained giant conductance enhancement in tunnel-coupled double quantum wires in a parallel magnetic field. The relative correction is found to be significant and depends on various effects such as the magnetic field, electron and impurity densities, impurity positions, symmetric and asymmetric doping profiles, and center barrier thickness.

PACS: 73.40.Gk, 72.20.My, 72.20.Fr, 73.40.Kp

DISCLAIMER

I. INTRODUCTION

In a recent letter, one of the authors proposed a giant low-temperature magneto-conductance mechanism in a closely tunnel-coupled double quantum wire structure.[1] The impurity-limited conductance was shown to be enhanced abruptly by as much as two orders of magnitude within a narrow range of an applied parallel magnetic field. The double quantum wires which are stacked in the z direction and extended along the y direction are created by adding a lateral confinement to $GaAs$ double quantum wells (QW's) in the x direction. The lateral confinement is achieved by depositing split metal gates on the front and back of the double QW's (DQWs) of widths L_z, which deplete the electrons underneath the gates when a negative voltage is applied. The thickness L_B of the $AlGaAs$ center barrier between the QW's is small (*e.g.*, $15 \sim 40$ $\mathring{A}$), allowing the electrons to tunnel in the z direction. In this paper, we consider an extreme size quantum limit where only the ground sub-level from the x-confinement and the ground tunnel-split doublet from the z-confinement are relevant. The magnetic field $\vec{B} = (B,\ 0,\ 0)$ is in the x direction. By using a two-dimensional finite-difference wave-packet technique, a recent numerical calculation[2] of coupled double wires with somewhat different numerical values for the QW depths, widths and the barrier widths yielded a much smaller conductance enhancement than predicted by the Born approximation,[1] making it necessary to examine the effects of higher-order corrections to the Born approximation which yielded the large enhancement. While we find that the corrections amount to as much as about 22% for short range impurity scattering, the conductance enhancement is still two to three orders of magnitude as predicted by Lyo.[1]

The basic idea of the conductance enhancement can be understood from the energy dispersion curves of symmetric double quantum wires at 4.8 T in Fig. 1. Here, the dash-dotted curves indicate the energy parabolas of the two QW's in the absence of tunneling, displaced relative to each other by the magnetic field in an amount of $\Delta k = d/\ell^2$ where d is the well to well separation and $\ell = (\hbar/eB)^{1/2}$ is the magnetic length. The degeneracy at the crossing point is removed due to tunneling, opening an anti-crossing gap which separates

the upper and lower branches shown by the solid curves. The gap moves up in energy as the diamagnetic energy increases with increasing B and crosses the chemical potential μ.[1] The chemical potential is shown by a horizontal dashed line in Fig. 1. The Born approximation for the momentum dissipation corresponds to the direct back scattering between the initial and final Fermi points k_i and k_f shown by the filled circles. In this case, the confinement wave functions at the two Fermi points are separated and localized in QW1 and QW2 with a very small overlap, yielding a very small scattering rate. In contrast, when μ is above the gap, we have two pairs of Fermi points such that the wave functions of the pairs have large amplitudes in QW1 and QW2, respectively, yielding a large scattering rate. Also, when μ is below the gap at a higher field, back scattering occurs inside the same QW as illustrated by the broken arrows in Fig. 1. Therefore, the scattering rate is relatively large when μ lies outside the gap. As a result, a giant conductance enhancement is obtained in the range of the magnetic field where μ is inside the gap.

The Born approximation may, however, underestimate the scattering rate when μ is inside the gap and overestimate the conductance enhancement. There are higher-order processes which give significant contributions to back scattering. These processes are illustrated in Fig. 1 by solid arrows. In these two-step processes, scattering occurs through the intermediate virtual states near the gap edges (*i.e.*, near $k = 0$) shown by the open circles. These intermediate states have large amplitudes in both QW's, providing a significant simultaneous overlap with the initial and final wave functions at k_i and k_f. In this paper, we study the effect of these higher-order contributions.

The organization of this paper is as follows. In Section II, we present the formalism beyond the Born approximation for the conductance of the electrons in the double quantum wires under a parallel magnetic field. Numerical results and discussions are presented in Sec. III for the relative corrections to the conductance enhancement introduced by the higher-order corrections as a function of magnetic field. The paper is concluded in Sec. IV with some brief remarks.

II. FORMALISM

Using the Landau gauge for the vector potential $\vec{A} = (0,\ -Bz,\ 0)$, the Hamiltonian of the system is given by $\hat{\mathcal{H}} = \hat{\mathcal{H}}_z + \hat{\mathcal{H}}_x$ with

$$\hat{\mathcal{H}}_z = -\frac{\hbar^2}{2}\,\frac{\partial}{\partial z}\left(\frac{1}{m_e^*(z)}\,\frac{\partial}{\partial z}\right) + V_{DQW}(z) + \frac{\hbar^2}{2m_e^*(z)}\left(k - \frac{z}{\ell^2}\right)^2 , \tag{1}$$

$$\hat{\mathcal{H}}_x = -\frac{\hbar^2}{2m_W}\,\frac{\partial^2}{\partial x^2} + V_L(x) , \tag{2}$$

where $m_e^*(z)$ is the position-dependent effective mass of electrons in the z-direction, which equals $m_W = 0.0665 m_0$ inside the $GaAs$ wells and $m_B = (0.0665 + 0.083\eta)m_0$ inside the $Al_\eta Ga_{1-\eta}As$ barriers with η being the alloy composition index of the ternary barrier material, m_0 is the free electron mass, $V_{DQW}(z) = 0.57 \times 1.427\eta$ (eV) in the barrier region and zero inside the well, and $V_L(x)$ is the lateral confinement potential of the quantum wires. Moreover, k in Eq. (1) is the electron wave vector along the wires. For the Hamiltonian in Eqs. (1) and (2), the electron wave functions can be written as

$$< \vec{r}|j, k >= \frac{1}{\sqrt{L_y}}\,\phi_0(x)\ \exp(iky)\ \psi_{jk}(z) , \tag{3}$$

where the electrons are assumed to be in the lowest energy eigen-state $\phi_0(x)$, and the index $j = 1,\ 2$ stands for the lower and upper tunnel-split branches in the z direction. The electron energy is given by

$$\mathcal{E}_{j\kappa} = E_0^x + E_j^z(k) , \tag{4}$$

where $E_j^z(k)$ is determined by $\hat{\mathcal{H}}_z\psi_{jk}(z) = E_j^z(k)\psi_{jk}(z)$, and E_0^x is the ground level given by $\hat{\mathcal{H}}_x\phi_0(x) = E_0^x\phi_0(x)$. As seen from the last term in Eq. (1), the effect of B is to displace the origins of the transverse crystal momenta k in the wire direction in the two quantum wells relative to each other by $\Delta k = d/\ell^2$. Here, $d = L_z + L_B$ is the center-to-center distance between QW's. The energy dispersion curves $E_j^z(k)$ are displayed in Fig. 1 for $\eta = 0.3$, $L_z = 80$ $\mathring{A}$, $L_B = 50$ $\mathring{A}$, and $B = 4.8$ T.

The conductance is given by

$$G(B) = \frac{2e^2}{L_y^2} \sum_{j,k} v_{jk} \ [-f'(\mathcal{E}_{jk})] \ g_{jk} \ , \tag{5}$$

where $v_{jk} = \hbar^{-1} dE_j^z(k)/dk$, $g_{jk} = v_{jk}\tau_{jk}$, and τ_{jk} is the relaxation time. The factor of 2 results from the spin summation. In Eq. (5), $f'(\mathcal{E}_{jk})$ is the first derivative of the Fermi function. The quantity g_{jk} represents the linear deviation from the equilibrium Fermi distribution and satisfies the Boltzmann equation:

$$v_{jk} - \frac{2\pi}{\hbar} \sum_{m,p} (g_{jk} - g_{mp}) \ \mathcal{I}_{jk,mp} \ \delta(\mathcal{E}_{jk} - \mathcal{E}_{mp}) = 0 \ , \tag{6}$$

where $\mathcal{I}_{jk,mp} = \mathcal{I}^{(0)}_{jk,mp} + \Delta\mathcal{I}_{jk,mp}$ is the irreducible scattering part shown in Fig. 2 (a) for the ladder approximation in the diagrammatic expansion of the current-current correlation function.[3] The first term $\mathcal{I}^{(0)}_{jk,mp}$, represented by a rung, is the Born approximation and is the impurity-averaged scattering strength times the total number of impurities N_I (see Eq. (9)) while the second term is the higher-order single-impurity correction. Although this term is of higher order in the scattering potential than the Born term, it occurs without a small direct overlap between the initial and final states in the gap. Instead, the final and initial states are mediated through the intermediate states which have large overlap with both states as discussed in Sec. I and as seen below in Eq. (12). Hence, we need not consider the third-order contributions shown in Fig. 2 (b) which include a direct overlap between the initial and final states. The conductance in Eq. (5) yields

$$G(B) = \frac{2e^2}{hL_y} \ g \ , \tag{7}$$

where g is the sum of g_{jk} over all the Fermi points. An exact solution for g was obtained in Ref. 1 and is given by replacing $V^2(k,\ p)$ in Eqs. (5)-(7) of Ref. 1 with $\mathcal{I}_{jk,mp}$. The relative correction to the Born conductance $G^{Born}(B)$ due to higher-order scattering $\Delta\mathcal{I}_{jk,mp}$ is

$$\frac{\Delta G}{G} = \frac{G^{Born}(B) - G(B)}{G(B)} \ . \tag{8}$$

The impurity interaction matrix in Eq. (6) is

$$\mathcal{I}^{(0)}_{jk,\ell s} = N_I \int d^3\vec{R}_\lambda \, \mathcal{P}(\vec{R}_\lambda) \, \left| u^\lambda_{jk,\ell s} \right|^2 , \tag{9}$$

where $\vec{R}_\lambda$ is the position of an individual impurity atom and $\mathcal{P}(\vec{R}_\lambda)$ is the probability density distribution function of the impurity atoms in the system with $\int d^3\vec{R}_\lambda \, \mathcal{P}(\vec{R}_\lambda) = 1$. The matrix element in Eq. (9) is given by

$$u^\lambda_{jk,mp} = \frac{1}{L_y} \int d^3\vec{r} \, U^{imp}(\vec{r} - \vec{R}_\lambda) \, \phi^2_0(x) \, \exp\left[i(p-k)y\right] \, \psi_{jk}(z)\psi_{mp}(z) , \tag{10}$$

where $U^{imp}(\vec{r} - \vec{R}_\lambda)$ is the interaction potential between the electron at $\vec{r}$ and the impurity atom at $\vec{R}_\lambda$. The higher-order scattering part in Eq. (6) is given by

$$\Delta\mathcal{I}_{jk,\ell s} = N_I \int d^3\vec{R}_\lambda \, \mathcal{P}(\vec{R}_\lambda) \, \left| T^\lambda_{jk,\ell s}(\mathcal{E}_{jk}) \right|^2 , \tag{11}$$

where $T^\lambda_{jk,\ell s}(\mathcal{E})$ includes only the principal part:

$$T^\lambda_{jk,\ell s}(\mathcal{E}) = \sum_{m,p} u^\lambda_{jk,mp} \, u^\lambda_{mp,\ell s} \, \frac{(\mathcal{E} - \mathcal{E}_{mp})}{[\mathcal{E} - \mathcal{E}_{mp}]^2 + [\Gamma_{mp}(\mathcal{E})]^2} . \tag{12}$$

Here, $\Gamma_{mp}(\mathcal{E})$ is the energy-dependent damping:

$$\Gamma_{jk}(\mathcal{E}) = \pi N_I \sum_{m,p} \int d^3\vec{R}_\lambda \, \mathcal{P}(\vec{R}_\lambda) \, \left| u^\lambda_{jk,mp} \right|^2 \, \delta(\mathcal{E} - \mathcal{E}_{mp}) . \tag{13}$$

III. NUMERICAL RESULTS AND DISCUSSIONS

In this section, we present numerical results for the B-dependent conductance enhancement. Several different structures of double quantum wires as well as doping configurations are studied to bring out salient features of the results. We assume that the impurities are distributed uniformly on several $\delta-$doping sheets perpendicular to the z direction:[4]

$$\mathcal{P}(Z_\lambda) = \left[C_1 \, \delta(Z_\lambda - z_1) + C_2 \, \delta(Z_\lambda - z_2) + \cdots\right] / \mathcal{S} , \tag{14}$$

where z_i is the impurity sheet position, $\mathcal{S}$ is the area of the impurity sheet and C_i is the fractional distribution with $C_1 + C_2 + \cdots = 1$. Mostly, we will study a binary distribution (*i.e.*, $C_1 + C_2 = 1$) for various positions of the impurity sheets. Next, we assume that the short-range screened electron-impurity interaction takes a Gaussian form[5]

$$U^{imp}(\vec{r}-\vec{R}_\lambda) = U_0 \ \exp\left[-\frac{|\vec{r}-\vec{R}_\lambda|^2}{\Lambda_0^2}\right] \ , \tag{15}$$

where the interaction strength is U_0 and Λ_0 measures the interaction range. Finally, we assume that the lateral confinement of the quantum wires takes a parabolic potential[6] $V_L(x) = m_W\Omega_x^2 x^2/2$, yielding

$$\phi_0(x) = \left(\frac{\alpha}{\sqrt{\pi}}\right)^{1/2} \exp\left(-\frac{1}{2}\,\alpha^2 x^2\right) \tag{16}$$

with $\alpha = \sqrt{m_W\Omega_x/\hbar}$. The interaction matrices in Eqs. (9) and (11) are then explicitly given by

$$\mathcal{I}^{(0)}_{jk,\ell s} = \frac{n_I\pi\alpha\Lambda_0^4U_0^2}{\sqrt{1+\alpha^2\Lambda_0^2}}\sqrt{\frac{\pi}{2}}\ \exp\left[-\frac{1}{2}(s-k)^2\Lambda_0^2\right]\ \sum_\beta C_\beta\ \left[W^\beta_{jk,\ell s}\right]^2 \ , \tag{17}$$

$$\Delta\mathcal{I}_{jk,\ell s} = \frac{n_I\pi^2\alpha^3\Lambda_0^8U_0^4}{L_y^2(1+\alpha^2\Lambda_0^2)^{3/2}}\ \frac{\sqrt{\pi}}{2}\ \sum_\beta C_\beta$$

$$\times\left\{\sum_{m,p}\exp\left(-\frac{1}{4}[(p-k)^2+(s-p)^2]\Lambda_0^2\right)\ \frac{(\mathcal{E}-\mathcal{E}_{mp})}{[\mathcal{E}-\mathcal{E}_{mp}]^2+[\Gamma_{mp}(\mathcal{E})]^2}\ W^\beta_{jk,mp}\ W^\beta_{mp,\ell s}\right\}^2 \ , \tag{18}$$

where $n_I = N_I/\mathcal{S}$ is the total two-dimensional impurity density of the system, and the impurity interaction integral is given by

$$W^\beta_{jk,mp} = \int\ dz\ \psi_{jk}(z)\psi_{mp}(z)\ \exp\left[-\frac{1}{\Lambda_0^2}(z-z_\beta)^2\right] \ . \tag{19}$$

In the following numerical calculations, we consider two samples. Sample 1 is the symmetric $Al_{0.3}Ga_{0.7}As/GaAs$ DQWs with 280 meV barrier heights, $L_z = 80$ $\AA$ well widths, and $\hbar\Omega_x = 265$ meV. The effective mass of electrons is $m_W = 0.067m_0$ ($m_B = 0.073m_0$) in the wells (barriers). The center barrier thickness is $L_B = 60$ $\AA$, and the tunneling gap at $B = 0$ is 0.8 meV. The impurity interaction strength is $U_0 = 1.26$ eV and the impurity interaction range is $\Lambda_0 = 12$ $\AA$. Sample 2 has the same parameters as those of sample 1 except that the center barrier thickness is $L_B = 50$ $\AA$ and the tunneling gap at $B = 0$

is 1.5 meV. The calculations are performed at $T = 4\ K$. Other parameters used in the calculation will be given in the corresponding figure captions.

In Fig. 3(a), we compare $G(B)/G(0)$ for sample 1. Note that while $G(B)/G(0)$ is independent of n_I in the Born approximation, higher-order contributions depend on n_I through the energy-dependent damping term in Eq. (13). The Born enhancement is shown in (a) by the dashed curve. A giant enhancement of the conductance is obtained when μ lies inside the anti-crossing gap in the range of the field between 4.2 T and 5.2 T. The effect of the higher-order correction in Fig. 3(a) can be as much as 22% as seen from Fig. 3(b). It is interesting to note that the effect of the higher-order correction is smaller for larger n_I in Fig. 3(b). This is due to the fact that back scattering through the intermediate states becomes suppressed, when the damping $\Gamma_{mp}(\mathcal{E}_{jk}) \propto n_I$ in the denominator of Eq. (12) becomes large. From Fig. 3(b) we find that $\Delta G/G$ is decreased by more than an order of magnitude when n_I is increased from $n_I = 8.12 \times 10^{10}\ cm^{-2}$ to $n_I = 8.12 \times 10^{11}\ cm^{-2}$. For the lower n_I in (b), the dips D_1 and D_2 at the edges of the gap come from the high density-of-states, which enhances $\Gamma_{mp}(\mathcal{E}_{jk})$ and suppresses $\Delta G/G$. The dip D_3 around the middle of the gap is due to the cancellation between the positive and negative contributions to the numerator $\mathcal{E} - \mathcal{E}_{mp}$ in Eq. (12) from the intermediate states near both edges of the gap. Small fluctuations in the curves in Fig. (3) are due to the numerical fluctuations arising from using a finite number of k points in the numerical evaluation.

In Fig. 4, we compare $G(B)/G(0)$ for sample 1 with different positions of $\delta-$doping sheets in the two outer barrier layers. When the two impurity sheets are moved by 15 $\AA$ from the outer interfaces of QW's into the barriers as shown in the inset, the enhancement $G(B)/G(0)$ is increased significantly inside the gap (*i.e.*, $4.2\ T < B < 5.2\ T$) although there is almost no change outside the gap. In this case, the impurity interaction in Eq. (19) is reduced when μ is inside the gap. This explains the increase of $G(B)/G(0)$ in the figure. $G(B)/G(0)$ is insensitive to Λ_0 for $12\ \AA \leq \Lambda_0 \leq 25\ \AA$. From Eqs. (17) and (18), the increase of Λ_0 enhances the impurity interaction matrix elements in Eq. (19) but suppresses the form

factors (*i.e.*, large momentum transfer) in Eqs. (17) and (18) at the same time, both outside and inside the gap. For this reason, the enhancement is largely insensitive to Λ_0.

$G(B)/G(0)$ is compared in Fig. 5 for symmetric and asymmetric doping of sample 1 for $n_I = 8.12 \times 10^{11}\ cm^{-2}$. By changing from symmetric to asymmetric doping, $G(B)/G(0)$ remains the same inside the gap but is increased outside the gap. Here, $\Delta G/G$ is very small as already discussed regarding Fig. 3 (b). The increased $G(B)/G(0)$ outside the gap for asymmetric doping can be explained in the following way.[1,7] Under a large B, the wave functions at the Fermi points become separated into either one of QW's resembling two parallel resistors with individual resistance R_0 and combined resistance $R_0/2$ for symmetric doping. For asymmetric doping, the resistance of the channels becomes $R_0 \pm \Delta R$, yielding a total resistance $(R_0^2 - \Delta R^2)/2R_0 < R_0/2$. This implies that the asymmetric doping with $\Delta R \neq 0$ has the smaller total resistance or the larger total conductance compared to that in the symmetric doping. Namely, more current flows through the channel with fewer impurities and a higher conductance, increasing the total conductance. However, at $B = 0$ and inside the gap, the conductance depends only on $C_1 + C_2$ (which equals 1), yielding the same enhancement inside the gap for symmetric and asymmetric doping.

We show in Fig. 6 the dependence of $G(B)/G(0)$ on the electron density n_{1D} for sample 1 assuming that the number of the impurities inside the effective width of the wires equals that of the electrons: $n_{1D} = L_x n_I$ where L_x is the confinement width in the x direction. When n_{1D} is decreased from $6.5 \times 10^5\ cm^{-1}$ to $3.5 \times 10^5\ cm^{-1}$, the onset of the gap-enhancement region is shifted from $B = 4.2\ T$ to $B = 1.8\ T$ due to the reduction of μ. The visible reduction of $G(B)/G(0)$ inside the gap for the lower density $n_{1D} = 3.5 \times 10^5\ cm^{-1}$ is a result of a large overlap between the wave functions of the two Fermi points due to the fact that the degree of the separation of the wave functions into the two QW's are smaller at low fields. In addition, the dispersion around the gap edges becomes flatter at low fields, increasing the density-of-states there and relatively sharpening the dip of $G(B)/G(0)$ at the gap edges.

The quantities $G(B)/G(0)$ and $\Delta G/G$ are compared for samples 1 and 2 in Fig. 7. The gap in (a) is much larger for sample 2 (with a thinner center barrier) due to greater electron tunneling. Also, the wave functions at the two Fermi points inside the gap have much larger overlap with the impurities, leading to the reduction of $G(B)/G(0)$ inside the gap. Increased electron tunneling diminishes $\Delta G/G$ outside the gap in (b) for $n_I = 8.12 \times 10^{10}\ cm^{-2}$. This reduction is caused by the enhanced damping arising from larger wave function overlap with the impurities.

In Fig. 8, we present $G(B)/G(0)$ for sample 1 for two cases where the impurities lie (1) at all four interfaces and (2) only at the two outer interfaces. The total number of impurities is the same for each case. For the case with the two impurity sheets at the outer interfaces, $G(B)/G(0)$ is large inside the gap compared with the other case with two additional impurity sheets. This is due to the enhanced impurity interaction in Eq. (19) at the center barrier.

In Fig. 9, we exhibit $G(B)/G(0)$ for sample 1 with different positions of the impurity sheets in the center barrier. When the two impurity sheets are moved inward symmetrically by 5 $\AA$ from the interfaces, the enhancement $G(B)/G(0)$ decreases significantly inside the gap but increases only by a small amount outside the gap. Because the eigenstates of the upper branch are independent of k and anti-symmetric at $B = 0$, the wave functions have only a small amplitude at the impurity sites near the center of the middle barrier. As a result, $G(0)$ is greatly increased when the two impurity sheets are pushed towards the center of the middle barrier. On the other hand, this anti-symmetry is absent at high fields when μ lies within the gap. Consequently, $G(B)/G(0)$ is reduced inside the gap mainly due to the large value of $G(0)$.

The enhancement $G(B)/G(0)$ is displayed in Fig. 10 for $GaAs/Al_{0.3}Ga_{0.7}As$ DQWs at $T = 4\ K$ for another set of parameters which simulates the scattering of electrons by interface roughness.[2] The parameters are $L_z = 80\ \AA$, $L_B = 40\ \AA$, and $n_{1D} = 6.5 \times 10^5\ cm^{-1}$. $\Lambda_0 = 15\ \AA$ is the correlation length, and the total equivalent density of interface roughness is given by $n_I = 1/\pi\Lambda_0^2 = 14.16 \times 10^{12}\ cm^{-2}$ with $C_1 = C_2 = C_3 = C_4 = 0.25$. Furthermore, we

assume two-monolayer fluctuation $\bar{\Delta} = 10\ \mathring{A}$, giving rise to the ground-sub-level fluctuation which is the equivalent interaction strength $U_0 = \bar{E}(2\bar{\Delta}/L_z) = 20\ meV$. Here $\bar{E} = 80\ meV$ is the average energy of the tunnel-split ground sub-levels. For this sample, the anti-crossing gap is large (*i.e.*, $2\ meV$) due to the thin center barrier which increases the coupling between the two quantum wires. The enhancement $G(B)/G(0)$ is greatly suppressed inside the gap in Fig. 10 compared with the results obtained for sample 1 (with a thicker center barrier) because of the large overlap of the wave functions at the interfaces. We note that the equivalent U_0 is two orders of magnitude lower in this case. Consequently, the contribution from $\Delta I_{jk,\ell s}$ term in Eq. (18) to $\Delta G/G$ is reduced by four orders of magnitude compared to Figs. 7 and 8. This leads to a very small $\Delta G/G$, which implies that the Born approximation is more accurate in this particular case. We also note that n_{1D} in Fig. 10 is smaller than that used by Vurgaftman and Meyer.[2] As is explained by Fig. 6, the increase of n_{1D} will enhance $G(B)/G(0)$ inside the gap.

IV. CONCLUSIONS AND REMARKS

The effect of higher-order corrections to the Born approximation was studied for the giant conductance enhancement in tunnel-coupled double quantum wires in a parallel magnetic field. The relative correction was found to be as much as 22%. The effects of multiple scattering and weak localization have been neglected. The effect of coulomb interaction on the electron energy levels has also been neglected. Various effects have been found to play a role in the conductance enhancement. These effects include the impurity sheet densities, linear electron density, positions of the impurity sheets, symmetric and asymmetric impurity distribution, and the center barrier thickness. The higher-order corrections consist of two-step back-scattering processes through the virtual intermediate states near the gap edges. These processes increase the overlap of the wave functions at the two Fermi points with the impurities inside the anti-crossing gap and reduce the conductance enhancement compared to the Born approximation. The magnitude of the damping of the the intermediate states

near the gap edges has been shown to affect significantly the relative higher-order correction to the Born approximation.

We have also examined the effect of the interface roughness scattering on the conductance enhancement for strongly-coupled wires. A much smaller conductance enhancement was obtained for a sample with a thinner center barrier. Higher-order corrections to the Born approximation were found to be negligible for this case. The sample used in our calculation has a much smaller linear electron density compared with that studied by Vurgaftman and Meyer.[2] The anti-crossing gap of their sample occurs at much higher magnetic fields. Although a direct comparison was not made, our results indicate that the enhancement is much larger than that obtained by these authors. It is difficult to compare the enhancement mechanisms considered in our paper and in Ref. 2, because the latter relies totally on a numerical method.

ACKNOWLEDGMENTS

Sandia is a multiprogram laboratory operated by Sandia Corporation, a Lockheed Martin Company, for the U.S. DOE under Contract No.DE-AC04-94AL85000.

REFERENCES

[1] S. K. Lyo, J. Phys: Condens. Matter **8**, L703 (1996). The quantity $u_{1-,2+}$ in the first parenthesis on the right hand side of *Eq.* (6) should read: $u_{1-,2-}$.

[2] I. Vurgaftman and J. R. Meyer, J. Appl. Phys. **82**, 3881 (1997).

[3] G. D. Mahan, "*Many-Particle Physics*" (Plenum Press, New York, 1981), Charpt. 7.1, pp. 591-622.

[4] K. Esfarjani and H. R. Glyde, Phys. Rev. B **41**, 1042 (1990).

[5] T. Ando, A. B. Fowler, and F. Stern: Rev. Mod. Phys. **54**, 437 (1982).

[6] A. S. Plaut, H. Lage, P. Grambow, D. Heitmann, K. von Klitzing, and K. Ploog, Phys. Rev. Lett. **67**, 1642 (1991).

[7] A. Palevski, F. Beltram, F. Capasso, L. N. Pfeiffer, and K. W. West, Phys. Rev. Lett. **65**, 1926 (1990).

FIGURES

FIG. 1. Energy dispersion curves $E_j^z(k)$ with $j = 1,\ 2$ at $B = 4.8\ T$ for $\eta = 0.3$, $L_z = 80\ \mathring{A}$, $L_B = 50\ \mathring{A}$ and a schematic illustration of the two-step back scattering processes. The dashed horizontal line represents the chemical potential μ at $T = 4\ K$ for $n_{1D} = 6.5 \times 10^5\ cm^{-1}$. The dash-dotted curves are the energy levels in the absence of electron tunneling between the two wires. The solid arrows indicate higher-order scattering processes through the intermediate states (open circles) near the anti-crossing gap edges between the initial and final states (filled circles) when μ lies inside the gap. The broken arrows represent the back scattering processes within the quantum wires when μ is below the gap.

FIG. 2. (a) Second order (left) and fourth order (right) irreducible scattering part. (b) These third order diagrams are not important for the reason described in the text.

FIG. 3. (a) $G(B)/G(0)$ and (b) $\Delta G/G$ of sample 1 as a function of B. In (a), $G^{Born}(B)/G^{Born}(0)$ (dashed curve) and $G(B)/G(0)$ are shown for $n_I = 8.12 \times 10^{11}\ cm^{-2}$ (dash-dotted curve) and $n_I = 8.12 \times 10^{10}\ cm^{-2}$ (solid curve). The black dots in the inset indicate the impurities at the outer interfaces of the two quantum wells with $C_1 = C_2 = 0.5$. In (b), $\Delta G/G$ are presented for $n_I = 8.12 \times 10^{11}\ cm^{-2}$ (dashed curve) and $n_I = 8.12 \times 10^{10}\ cm^{-2}$ (solid curve), respectively. $T = 4\ K$, $n_{1D} = 6.5 \times 10^5\ cm^{-1}$ are assumed. The symbols D_1, D_2, and D_3 indicate the dips of $\Delta G/G$ at the edges of the gap and around the middle of the gap.

FIG. 4. $G(B)/G(0)$ and $G^{Born}(B)/G^{Born}(0)$ of sample 1 at $T = 4\ K$ as a function of B for two different positions of symmetric $\delta-$impurity sheets with $C_1 = C_2 = 0.5$. The impurity sheets are at the outer interfaces (dash-dotted curve) and 15 $\mathring{A}$ away from the outer interfaces inside the barriers (solid and dashed curves) as illustrated in the insets. Here, $n_I = 8.12 \times 10^{11}\ cm^{-2}$ and $n_{1D} = 6.5 \times 10^5\ cm^{-1}$.

FIG. 5. $G(B)/G(0)$ and $G^{Born}(B)/G^{Born}(0)$ of sample 1 at $T = 4\ K$ as a function of B for symmetric and asymmetric impurity distributions illustrated in the insets. The two impurity sheets are at the outer interfaces of the double quantum wells. Here, $C_1 = C_2 = 0.5$ for the symmetric impurity distribution (dash-dotted curve) and $C_1 = 0.6$ and $C_2 = 0.4$ for the asymmetric case (dashed and solid curves). The one-dimensional impurity density equals $n_{1D} = 6.5 \times 10^5\ cm^{-1}$ with $n_I = 8.12 \times 10^{11}\ cm^{-2}$.

FIG. 6. $G(B)/G(0)$ of sample 1 as a function of B for $n_{1D} = 6.5 \times 10^5\ cm^{-1}$ (dash-dotted curve) and $n_{1D} = 3.5 \times 10^5\ cm^{-1}$ (solid curve) at $T = 4\ K$. The dashed curve represents $G^{Born}(B)/G^{Born}(0)$ for $n_{1D} = 3.5 \times 10^5\ cm^{-1}$. The electron density is the same as that of impurities. The two impurity sheets are 15 $\AA$ away from the outer interfaces of the double quantum wells inside the barriers with $C_1 = C_2 = 0.5$.

FIG. 7. (a) $G(B)/G(0)$ and (b) $\Delta G/G$ of sample 1 and sample 2 as a function of B for $T = 4\ K$, $n_{1D} = 6.5 \times 10^5\ cm^{-1}$ and $n_I = 8.12 \times 10^{10}\ cm^{-2}$. In (a), $G(B)/G(0)$ of sample 1 (dash-dotted curve) is compared with $G^{\rm Born}(B)/G^{\rm Born}(0)$ (dashed curve) and $G(B)/G(0)$ (solid curve) of sample 2. In (b), $\Delta G/G$ is displayed for sample 1 (dash-dotted curve) and sample 2 (solid curve). In (a) and (b), the two impurity sheets are at the outer interfaces of the double quantum wells with $C_1 = C_2 = 0.5$ as illustraded in the insets of (a). The symbols D_1, D_2, and D_3 in (b) indicate the dips of $\Delta G/G$ at the edges of the gap and around the middle of the gap.

FIG. 8. $G(B)/G(0)$ and $G^{Born}(B)/G^{Born}(0)$ of sample 1 at $T = 4\ K$ for $n_{1D} = 6.5 \times 10^5\ cm^{-1}$ and $n_I = 8.12 \times 10^{10}\ cm^{-2}$ as a function of B. The insets show two different impurity configurations, namely $C_1 = C_2 = 0.5$ with the impurities at the outer interfaces only (dsah-dotted curve) and $C_1 = C_2 = C_3 = C_4 = 0.25$ with the impurities at the four interfaces (dashed and solid curves).

FIG. 9. $G(B)/G(0)$ and $G^{Born}(B)/G^{Born}(0)$ of sample 1 as a function of B at $T = 4\ K$ for $n_{1D} = 6.5 \times 10^5\ cm^{-1}$ and $n_I = 8.12 \times 10^{10}\ cm^{-2}$ for two different impurity positions in the center barrier. The impurities are at the interfaces (dash-dotted curve) and 5 $\AA$ away from the interfaces inside the barrier (dashed and solid curves) as illustrated in the insets.

FIG. 10. $G(B)/G(0)$ as a function of B at $T = 4\ K$ with an equal (*i.e.*, $C_1 = C_2 = C_3 = C_4 = 0.25$) impurity distribution (or interface roughness) at all four interfaces as illustrated in the inset. The parameters used are $\Lambda_0 = 15\ \AA$, $U_0 = 20\ meV$, $L_B = 40\ \AA$, $n_I = 1.416 \times 10^{13}\ cm^{-2}$, $L_z = 80\ \AA$, and $n_{1D} = 6.5 \times 10^5\ cm^{-1}$. Here, $G^{Born}(B)/G^{Born}(0)$ (dashed curve) and $G(B)/G(0)$ (solid curve) are nearly equal.

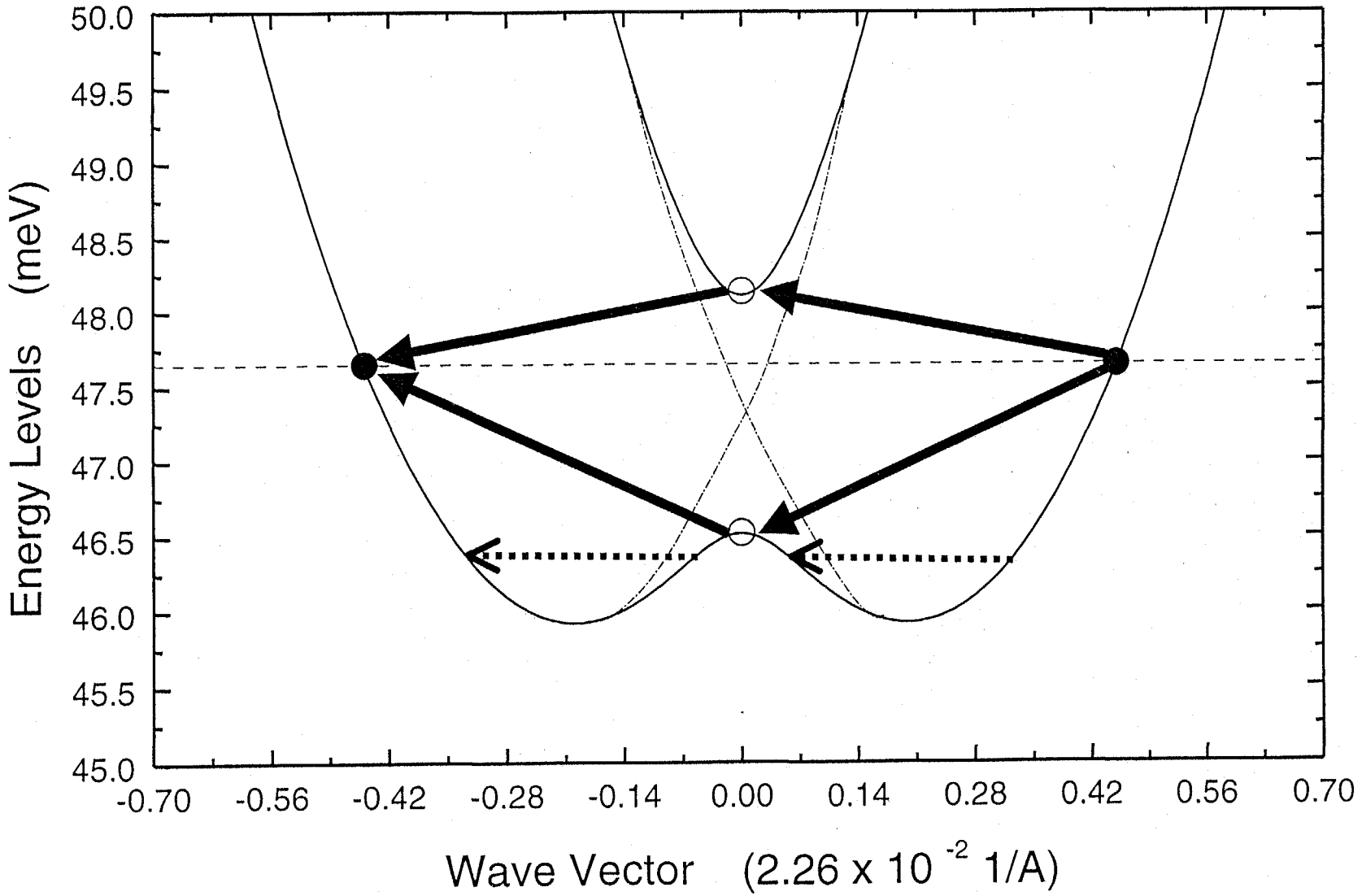
50.0
49.5
49.0
48.5
48.0
47.5
47.0
46.5
46.0
45.5
45.0
Energy Levels (meV)
-0.70
-0.56
-0.42
-0.28
-0.14
0.00
0.14
0.28
0.42
0.56
0.70
Wave Vector (2.26 x 10 -2 1/A)

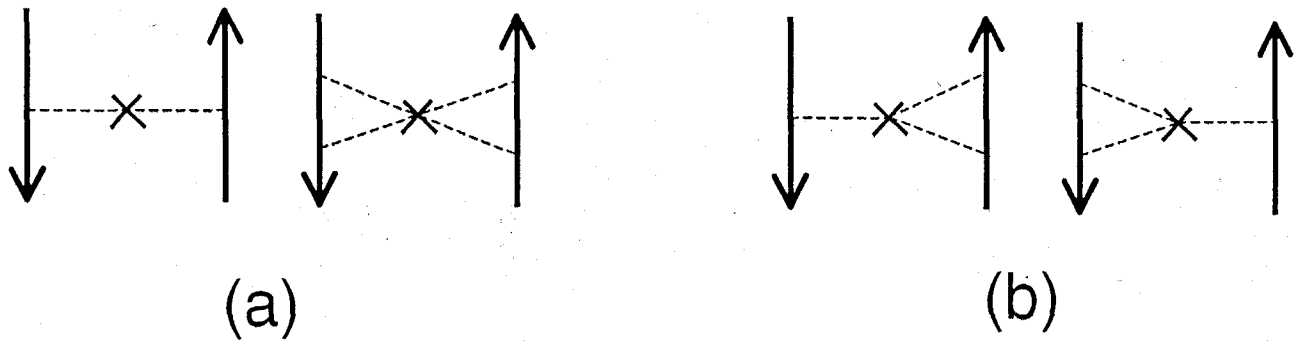
(a)
(b)

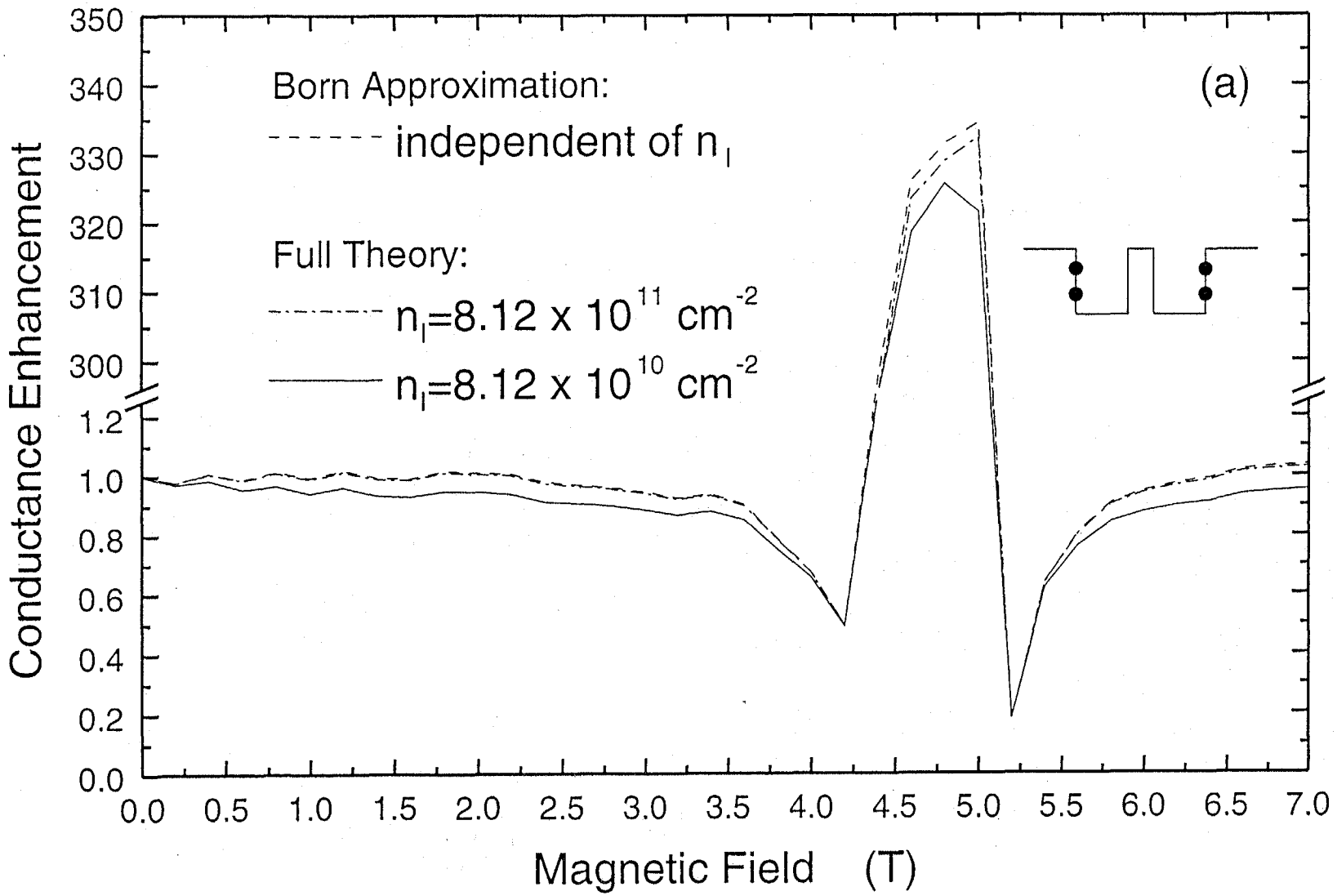
Born Approximation:
independent of n_I
Full Theory:
n_I=8.12 x 10^{11} cm^{-2}
n_I=8.12 x 10^{10} cm^{-2}
(a)
Conductance Enhancement
Magnetic Field (T)
350
340
330
320
310
300
1.2
1.0
0.8
0.6
0.4
0.2
0.0
0.0 0.5 1.0 1.5 2.0 2.5 3.0 3.5 4.0 4.5 5.0 5.5 6.0 6.5 7.0

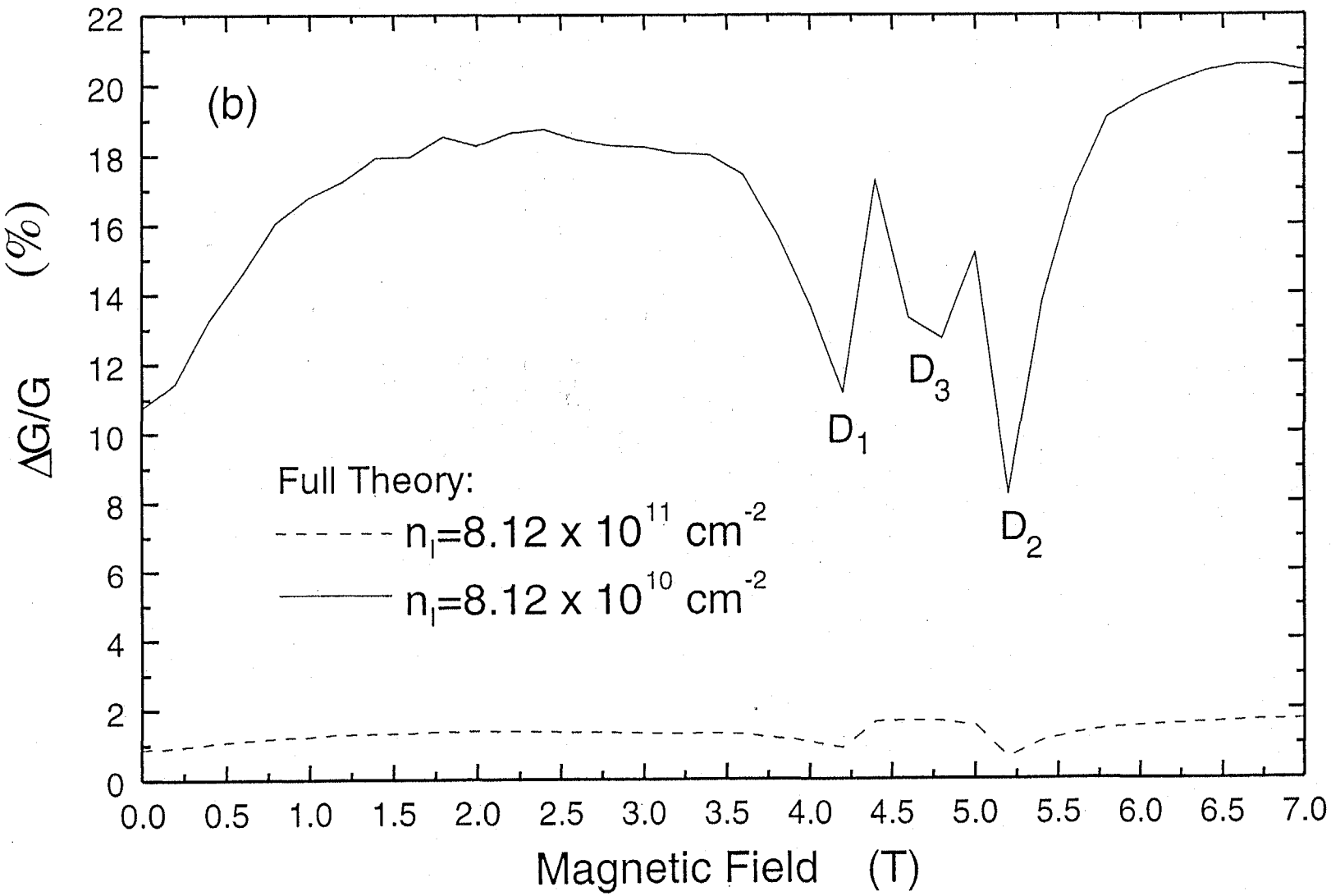
(b)
ΔG/G (%)
Magnetic Field (T)
Full Theory:
n_I=8.12 x 10^11 cm^-2
n_I=8.12 x 10^10 cm^-2
D1
D2
D3
0
2
4
6
8
10
12
14
16
18
20
22
0.0
0.5
1.0
1.5
2.0
2.5
3.0
3.5
4.0
4.5
5.0
5.5
6.0
6.5
7.0

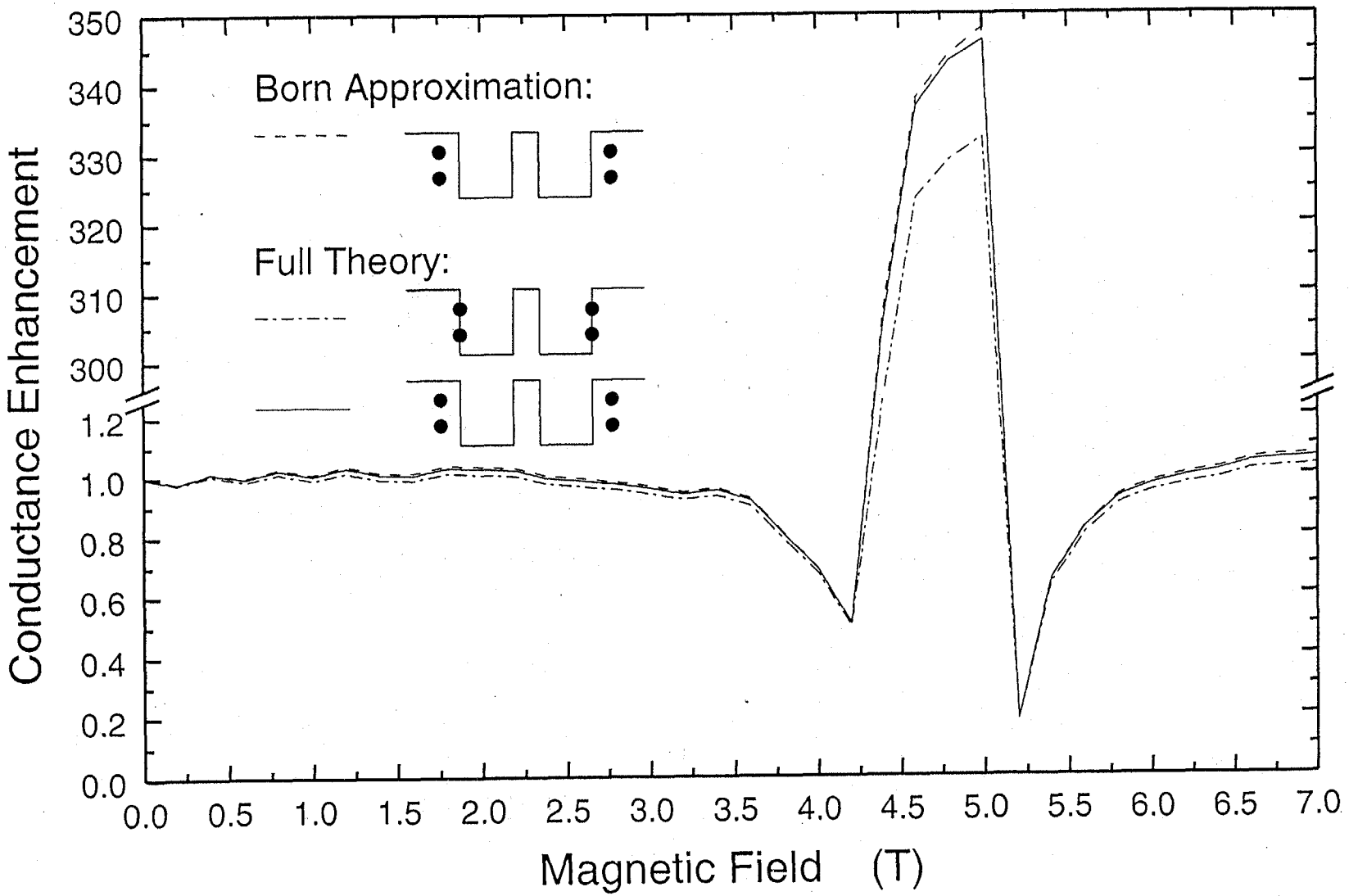
Born Approximation:
Full Theory:
Conductance Enhancement
Magnetic Field (T)
350
340
330
320
310
300
1.2
1.0
0.8
0.6
0.4
0.2
0.0
0.0
0.5
1.0
1.5
2.0
2.5
3.0
3.5
4.0
4.5
5.0
5.5
6.0
6.5
7.0

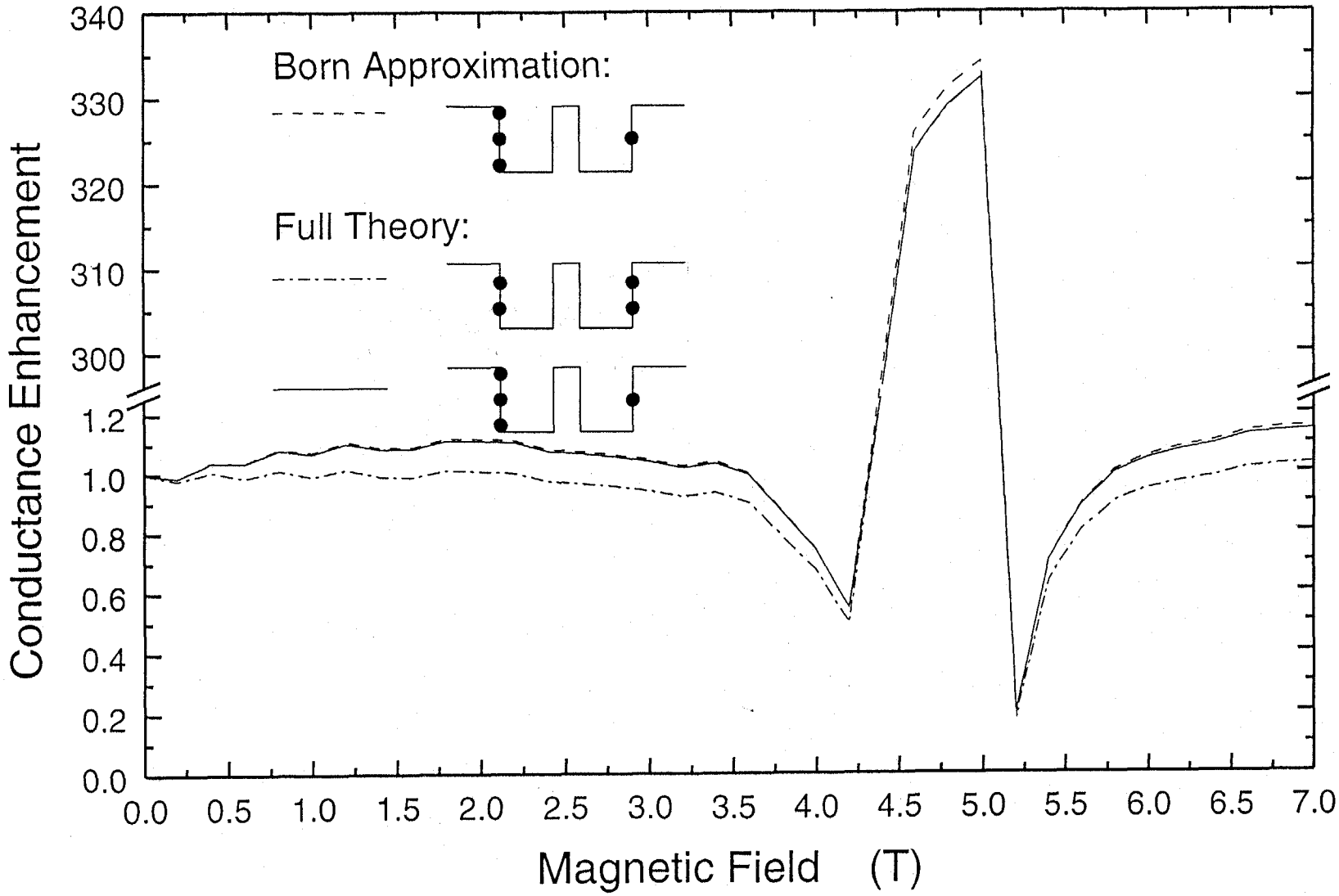
Born Approximation:
Full Theory:
Conductance Enhancement
Magnetic Field (T)
340
330
320
310
300
1.2
1.0
0.8
0.6
0.4
0.2
0.0
0.0
0.5
1.0
1.5
2.0
2.5
3.0
3.5
4.0
4.5
5.0
5.5
6.0
6.5
7.0

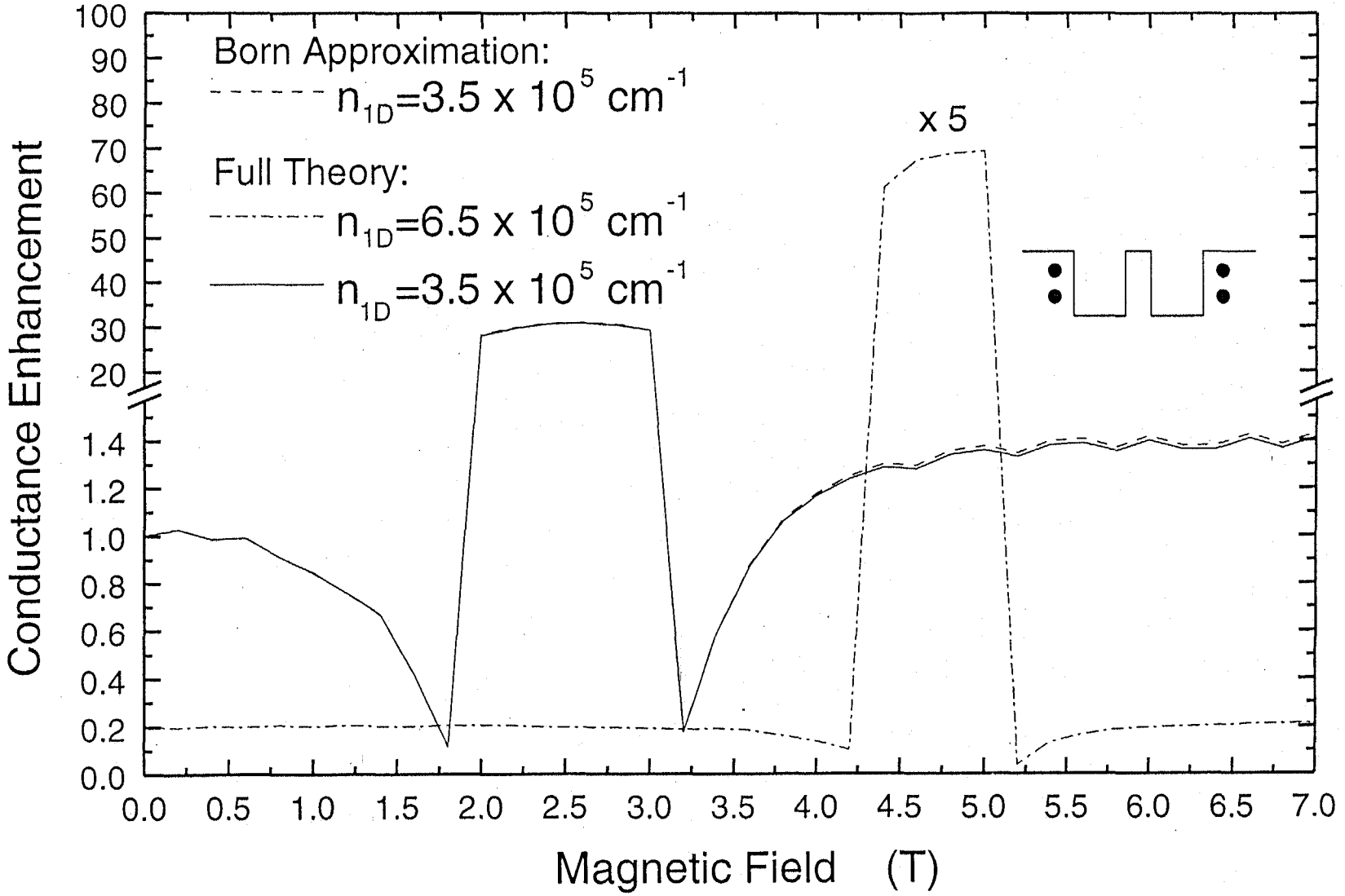
Born Approximation:
$n_{1D}=3.5 \times 10^5$ cm^{-1}
Full Theory:
$n_{1D}=6.5 \times 10^5$ cm^{-1}
$n_{1D}=3.5 \times 10^5$ cm^{-1}
x 5
Conductance Enhancement
Magnetic Field (T)
100
90
80
70
60
50
40
30
20
1.4
1.2
1.0
0.8
0.6
0.4
0.2
0.0
0.0 0.5 1.0 1.5 2.0 2.5 3.0 3.5 4.0 4.5 5.0 5.5 6.0 6.5 7.0

Huang et al. Fig. 7(a)

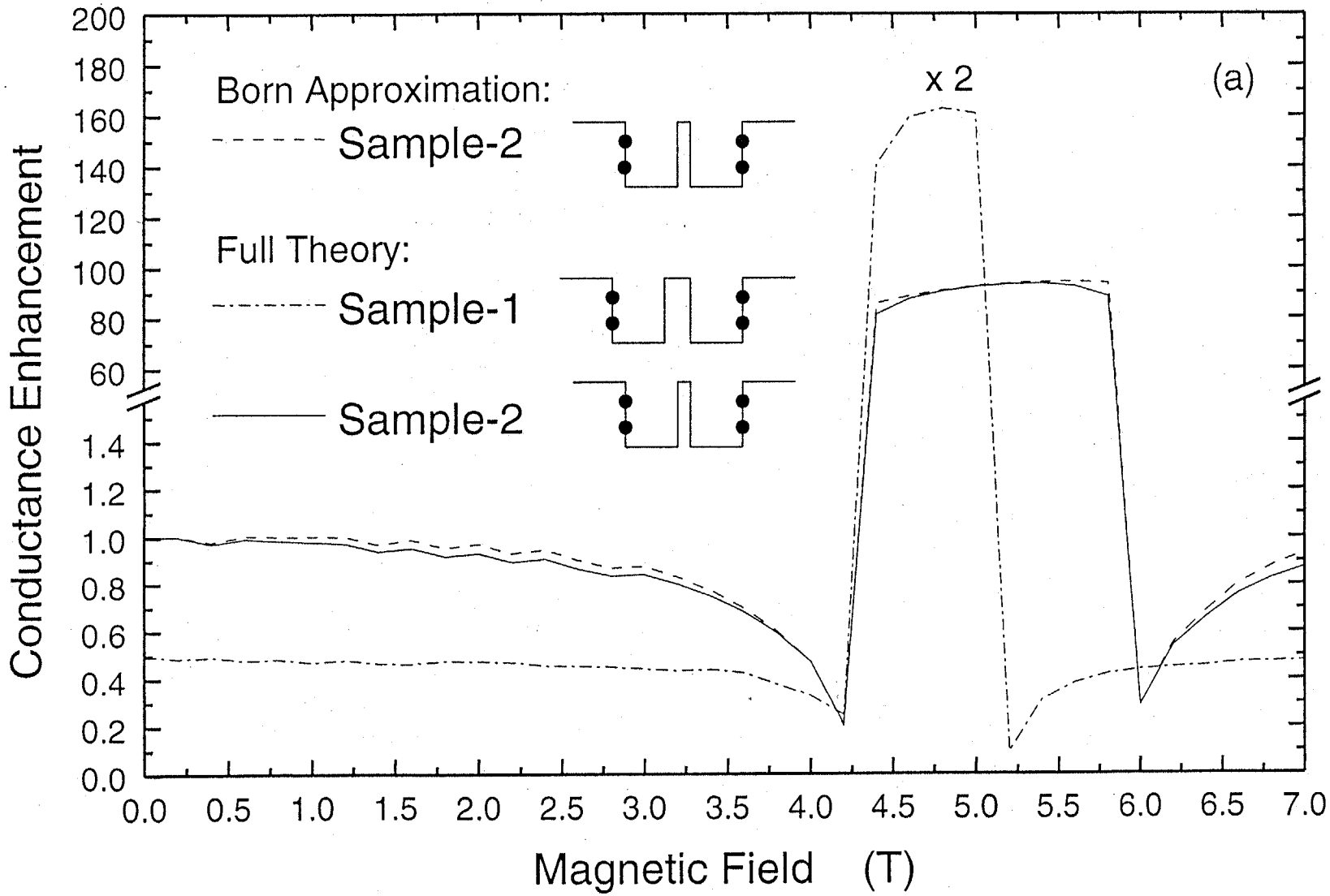

Huang et al. Fig. 7(b)

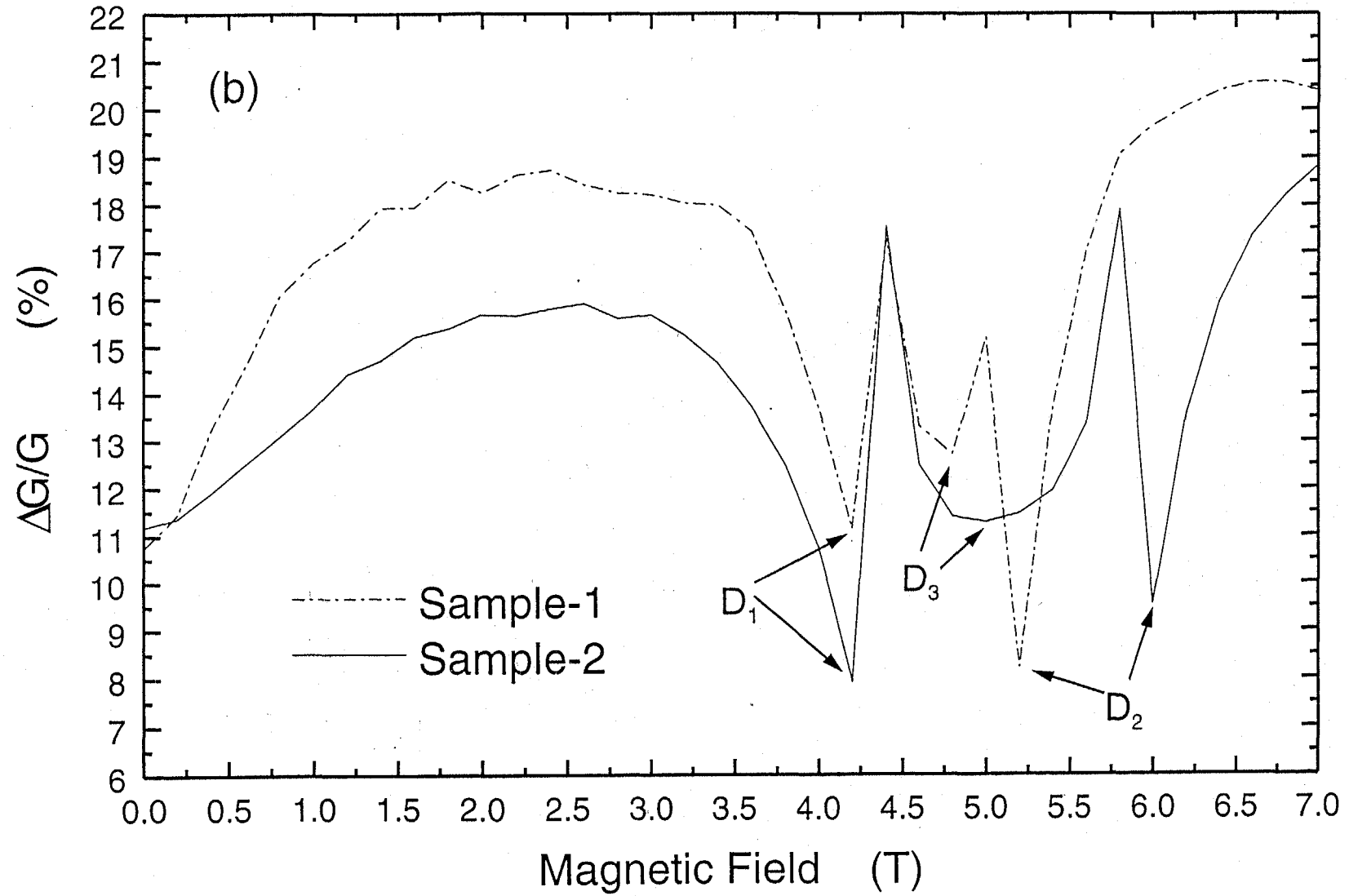

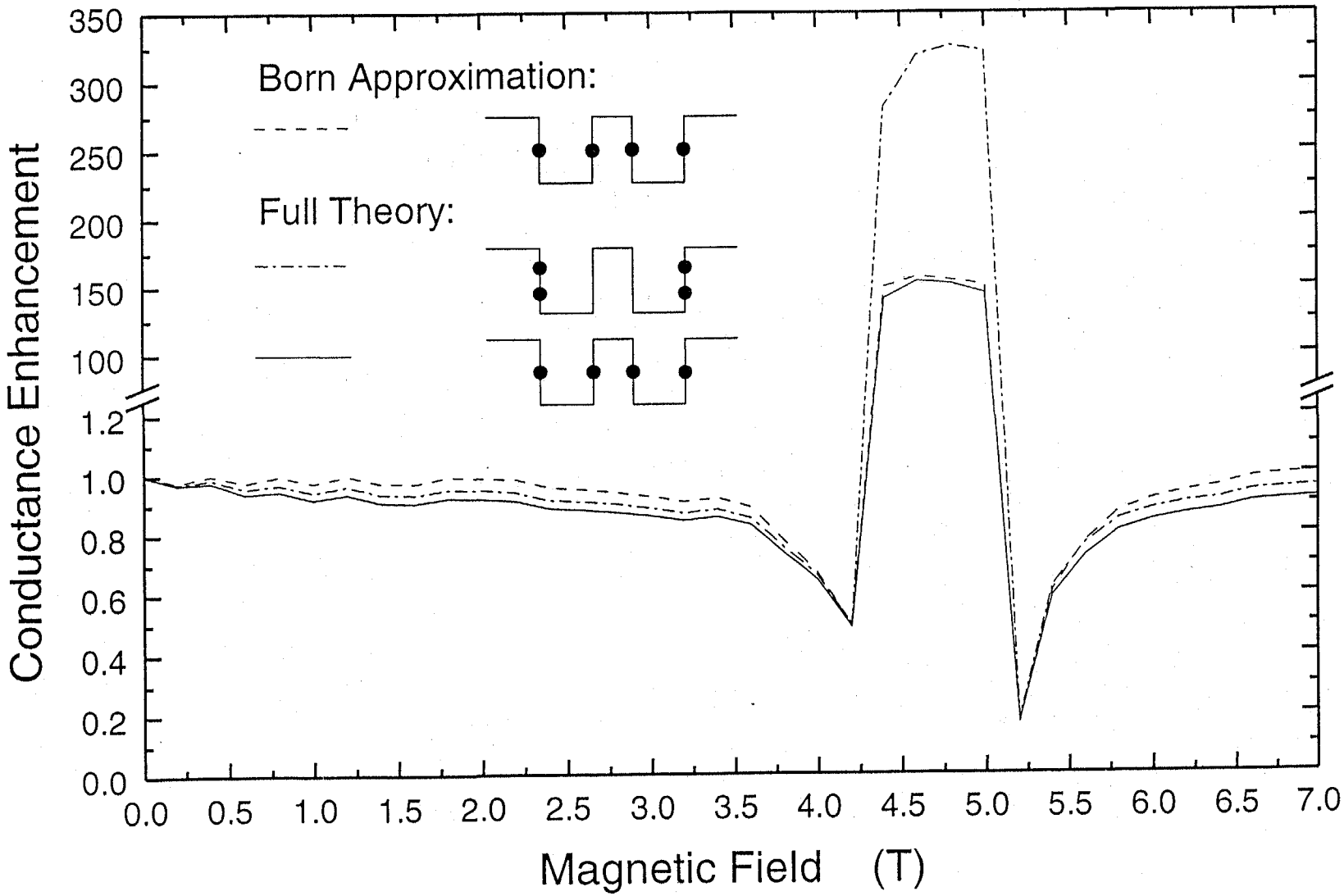
Born Approximation:
Full Theory:
Conductance Enhancement
Magnetic Field (T)
350
300
250
200
150
100
1.2
1.0
0.8
0.6
0.4
0.2
0.0
0.0
0.5
1.0
1.5
2.0
2.5
3.0
3.5
4.0
4.5
5.0
5.5
6.0
6.5
7.0

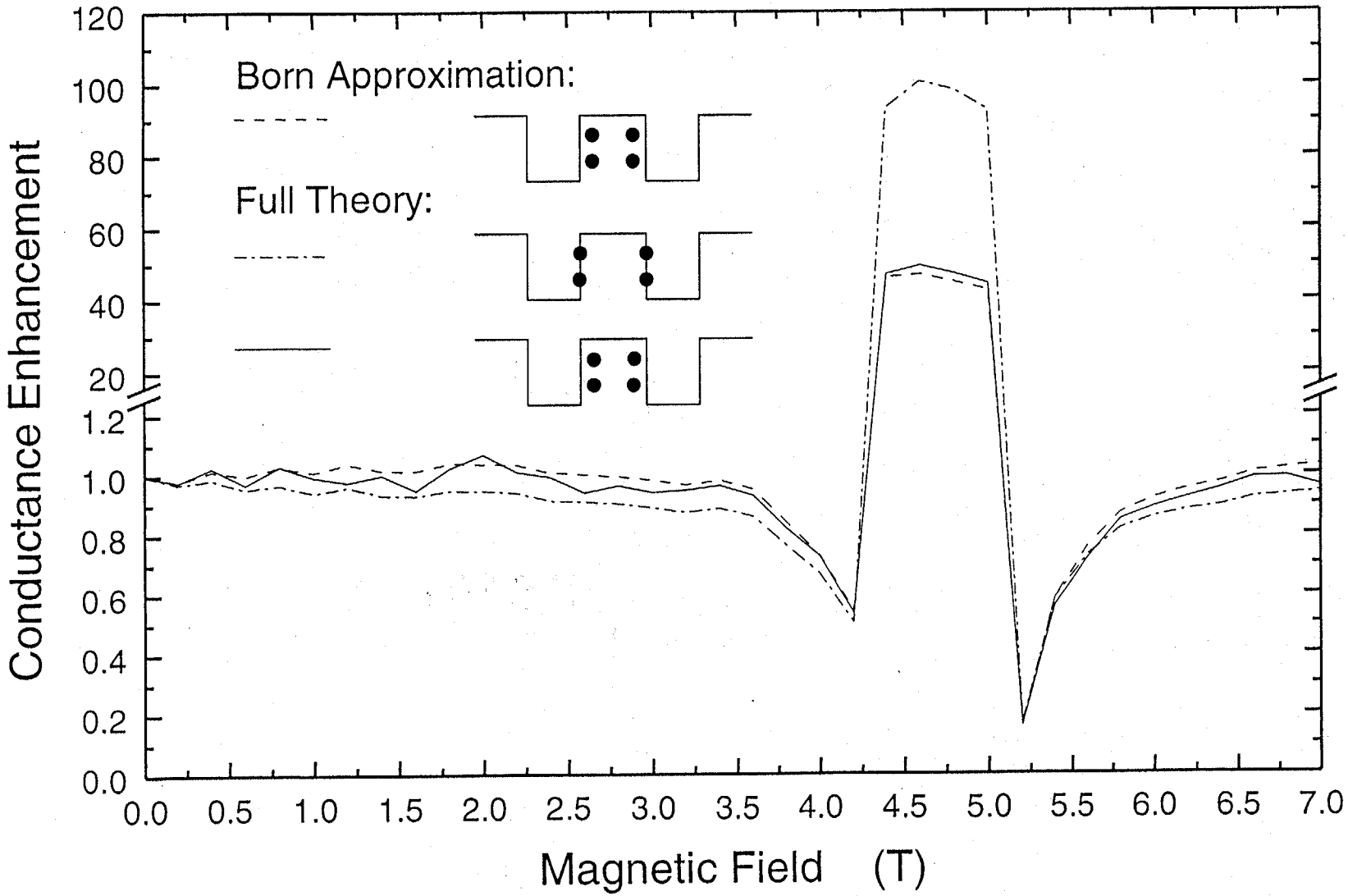
Born Approximation:
Full Theory:
Conductance Enhancement
Magnetic Field (T)
120
100
80
60
40
20
1.2
1.0
0.8
0.6
0.4
0.2
0.0
0.0
0.5
1.0
1.5
2.0
2.5
3.0
3.5
4.0
4.5
5.0
5.5
6.0
6.5
7.0

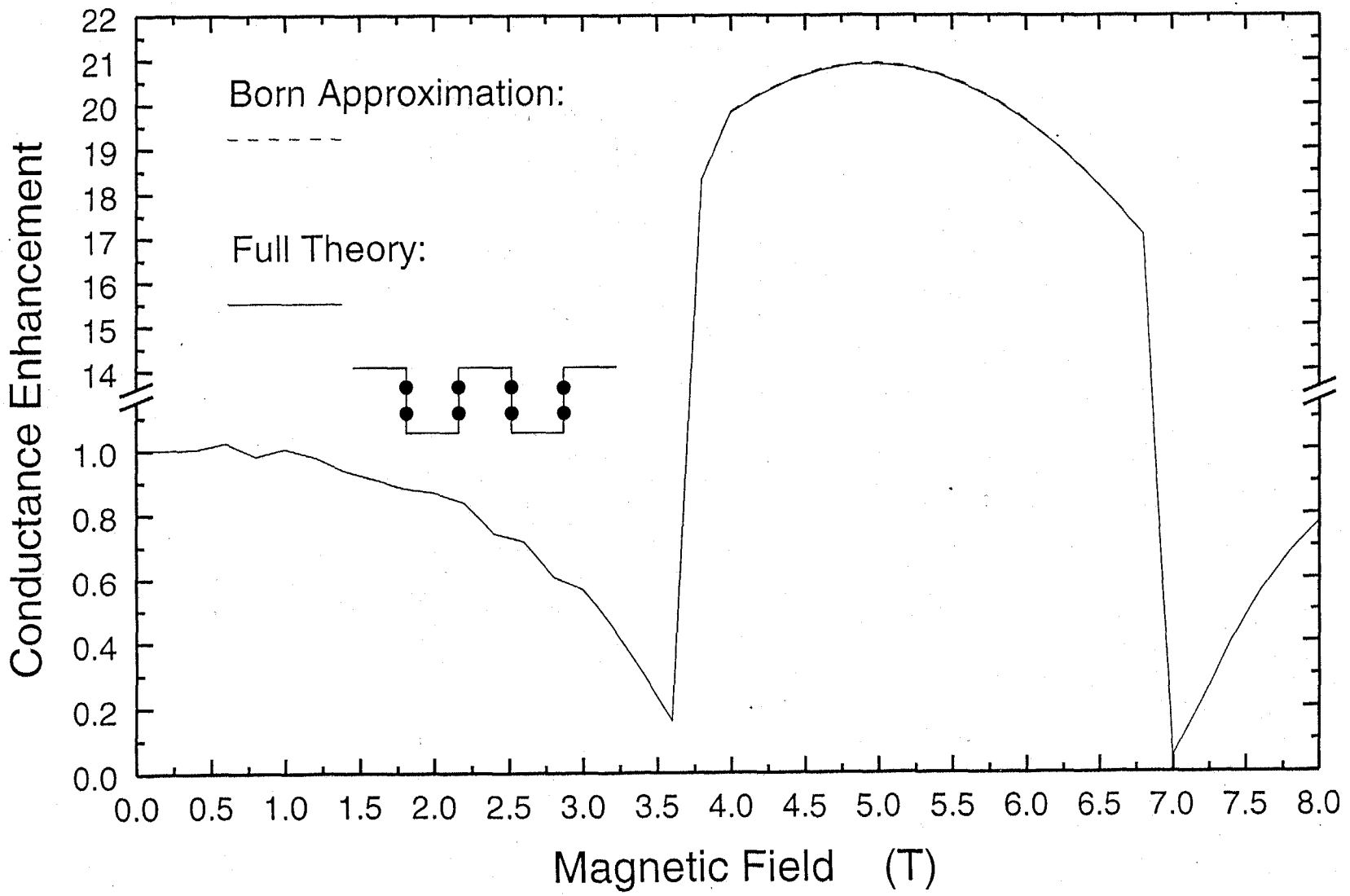
Born Approximation:
Full Theory:
Conductance Enhancement
Magnetic Field (T)
22
21
20
19
18
17
16
15
14
1.0
0.8
0.6
0.4
0.2
0.0
0.0 0.5 1.0 1.5 2.0 2.5 3.0 3.5 4.0 4.5 5.0 5.5 6.0 6.5 7.0 7.5 8.0